CHINA FOUNDRY Research & Development
Vol. 22 No. 4 July 2025
www.springer.com/41230
https://doi.org/10.1007/s41230-025-4144-8

Effects of Al and C content on κ-carbide precipitation and strengthening in high-Mn low-density steels: A quantitative study

Yu-xiang Liu[1], Tao Xu[1], *Jian-lei Zhang[1,2], Feng-hui An[3], Gang Chen[4], **Chang-jiang Song[1], and Qi-jie Zhai[1]

1. Center for Advanced Solidification Technology (CAST), School of Materials Science and Engineering, Shanghai University, Shanghai 200444, China

2. Shanghai Engineering Research Center for Integrated Circuits and Advanced Display Materials, Shanghai University, Shanghai 200444, China

3. Jiujiang Engineering Research Center of Advanced Welding, Jiujiang University, Jiujiang 332005, Jiangxi, China

4. Ningbo Branch of Chinese Academy of Ordnance Science, Ningbo 315103, Zhejiang, China

Abstract: Fe-28Mn-(10–12)Al-(0.8–1.4)C (wt.%) steels were designed to investigate the influence of varying Al and C content on precipitation behavior of κ-carbide and its contribution to the strength of high-Mn low-density steels. Results reveal that both Al and C elements promote κ-carbide precipitation, with C having a more pronounced effect. In near-rapidly solidified 10Al steel strips, increasing C content from 0.8wt.% to 1.4wt.% raises the κ-carbide size from 9.6 nm to 38.2 nm, accompanied by volume fraction increase from 10.2vol.% to 29.8vol.%. In comparison, the average size and volume fraction of κ-carbides in 12Al0.8C steel are only 11.4 nm and 17.8vol.%, respectively. Higher Al and C content reduces the lattice mismatch between austenite and κ-carbides, thus promoting nucleation of κ-carbides. Notably, the increase in C content results in a greater reduction in the Gibbs free energy of κ-carbide, leading to a stronger driving force for κ-carbide formation. Consequently, as the C content increases from 0.8wt.% to 1.4wt.%, the interaction between κ-carbides and dislocations transforms from particle cutting to bypassing, and the maximum precipitation strengthening of κ-carbides reaches 583 MPa. The construction of the relationship between Al and C content and κ-carbide precipitation in this study would provide valuable insights for alloy design of high-Mn steels.

Keywords: low-density steel; κ-carbide; Al and C content; precipitation strengthening

CLC numbers: TG142.3 **Document code:** A **Article ID:** 1672-6421(2025)04-480-13

1 Introduction

Fe-Mn-Al-C system steels are characterized by excellent comprehensive mechanical properties and low density, which have received extensive attention in automotive applications [1-5]. The addition of Al has been shown to significantly reduce steel's density, with reports suggesting that a 12wt.% Al addition could lead to an 18% density reduction [6]. Generally, the high content of Mn and C in low-density steels results in a single-phase austenitic structure or a dual-phase structure with a small amount of ferrite in austenitic matrix, thereby achieving excellent mechanical properties and deformability [7-10]. In austenitic low-density steels, the precipitation of κ-carbide, with a nominal stoichiometry of $(Fe, Mn)_3AlC$, plays a crucial role as a strengthening phase, contributing significantly to the overall strength of steels [11, 12]. Han et al. [13] demonstrated that dispersion of nano-scale intragranular κ-carbide could result in a strength increase of 200–500 MPa. Moreover, the coherent relationship between nano-scale κ-carbide and austenitic matrix can facilitate dislocations to cut through the κ-carbide, which in turn reduces dislocation pile-up and stress concentration. This process effectively enhances the yield strength of low-density steel while maintaining its plasticity [14, 15].

***Jian-lei Zhang**

Ph. D., Postdoctor. His research interests mainly focus on the development of advanced steels with metastable solidification. He has supervised 5 projects and published more than 20 papers in the field of steels.

E-mail: jianleizhang@shu.edu.cn

****Chang-jiang Song**

Ph. D., Professor. His research interests mainly focus on metal theory and microstructure control, and the development of super-performance metastable engineering materials through solidification process control. He has supervised over 20 projects and published more than 100 papers in international journals.

E-mail: riversong@shu.edu.cn; riversxiao@163.com

Received: 2024-07-11; Revised: 2024-09-25; Accepted: 2024-12-16

The regulation of κ-carbide precipitation and growth in low-density steels is mainly achieved by appropriate heat treatment processes and alloy composition design. Research has indicated that κ-carbides typically form in high-Mn low-density steels within a temperature range of approximately 400–750 °C [16-20]. An et al. [21] conducted aging treatments at 500 °C for 1 h and 700 °C for 1 h on Fe-29.8Mn-7.65Al-1.11C low-density steel, resulting in κ-carbide growth from 2 nm to around 20 nm and 35 nm, respectively. In fact, the formulation of heat treatment processes to regulate κ-carbide precipitation is based on the alloy composition of low-density steels, particularly the Al and C elements and their thermodynamic properties. It has been reported that in high-Mn low-density steels, the κ-carbides tend to form when the Al content exceeds 7wt.% and the C content is above 0.7wt.% [6]. Chin et al. [22] have established a correlation between Al content and the precipitation behavior of κ-carbides in Fe-30Mn-Al-C (wt.%) low-density steels by thermodynamic calculations. With increasing the Al content from 5wt.% to 11wt.%, the onset precipitation temperature of κ-carbide during the cooling process was increased from 680 °C to 900 °C. Furthermore, an increase in the C content from 0.4wt.% to 1.1wt.% resulted in coarsening of intragranular and intergranular κ-carbide in Fe-20Mn-8Al-C (wt.%) steels, leading to an intergranular fracture and a sharp decrease in impact absorption energy [23]. Wu et al. [24] found that in Fe-26Mn-*x*Al-1C (wt.%) low-density steels, an increase in Al content caused the size of the κ-carbide to increase from approximately 10 nm to 20 nm. The increase in size promoted the strain softening effect during plastic deformation, reduced the density of slip bands, and led to a continuous decrease in strain hardening rate of the low-density steels.

Additionally, the Mn content is a crucial factor affecting the solid solubility of Al and C elements and the formation of κ-carbides in low-density steels [25-29]. Generally, higher Mn content leads to increased solid solubility of Al and C in the austenitic matrix [25]. Furthermore, it raises the formation energy of κ-carbide, thereby inhibiting the growth and coarsening of κ-carbides [22]. Consequently, high-Mn low-density steels with elevated Al and C content, along with dispersed nano-scale κ-carbides, would be prone to achieve lower density and superior comprehensive mechanical properties. Wang et al. [30] found that an increase in C could significantly promote the precipitation of κ-carbides in Fe-30Mn-11Al-*x*C steels, while also increasing the yield strength from 800 MPa to 1,200 MPa. Ren et al. [31] found that the high Al content could promote the formation of DO_3 phase and κ-carbides in Fe-30Mn-11Al-1.2C steels, enhancing the yield strength from 520 MPa to 1,120 MPa, while also increasing the strain hardening rate. Studies have indicated that every 0.1wt.% C element increased the yield strength by 40 MPa, and every 1.0wt.% Al element raised the stacking fault energy by 11.3 $mJ \cdot m^{-2}$, demonstrating that increase in the content of Al and C elements resulted in an enhancement of yield strength and the transformation of deformation behavior [32,33]. Despite extensive research that has delved into regulating the precipitation of the κ-carbide in high-Mn low-density steels, the investigations predominantly focus on the impact of additional alloying elements (such as Cr, Mo, V, etc.), rather than the primary alloying elements [34-36]. The systematic calculation and analysis are deficient on the regulation of κ-carbide precipitation and the corresponding mechanical properties in high-Mn low-density steels, through variations in the content of the primary alloying elements Al and C.

This work focused on the effects of varying Al and C content on the precipitation behavior of κ-carbide and its strengthening effect on the Fe-Mn-Al-C low-density steel with a Mn content of 28wt.% under near-rapid solidification. Transmission electron microscope (TEM) was employed to quantitatively analyze the κ-carbide precipitation in high-Mn low-density steels. First-principles and thermodynamic calculations were utilized to elucidate the impact mechanism of Al and C content on the precipitation behavior of κ-carbides. Furthermore, the strength contribution of κ-carbides with different sizes was quantitatively analyzed in detail.

2 Experimental procedure

For the high-Mn austenite-based low-density steels, the minimum Al content necessary for κ-carbide precipitation is widely considered as 7wt.% [6], and the setting of Al content in high-Mn low-density steels is generally above 9wt.% [37]. However, the high content of Al would result in too much ferrite [38], changing the phase constitution of steels significantly. Therefore, the Al content of low-density steels in this work was set to 10wt.%–12wt.%. The Fe-28Mn-*x*Al-*y*C (wt.%, same as below) low-density steels were prepared using induction melting, where x=10, 11, or 12, and y=0.8, 1.0, 1.2, or 1.4. Initially, a 100 g alloy ingot was produced from high-purity Fe (99.99%), Mn (99.9%), Al (99.9%), and C (99.8%) using a cold-crucible suspension induction melting apparatus. Subsequently, the alloy ingot underwent induction melting again and was poured into a copper mold, rotating at 600 rpm under an Ar atmosphere, resulting in a near-rapidly solidified steel strip with dimensions of (60–80) mm×60 mm×2.5 mm. For simplicity, the low-density steels with varying Al and C content were named accordingly. For example, the steel with 10wt.% Al and 0.8wt.% C was named as 10Al0.8C steel.

The chemical compositions of the low-density steels were assessed using a CS2800 carbon-sulfur analyzer and inductively coupled plasma mass spectrometry (ICP), as detailed in Table 1. The density of the steel was determined through an SJ-600G electronic water displacement density analyzer, with the results also presented in Table 1. To identify the phase constitution of steels, an X-ray diffractometer (XRD, D/Max-2200, Cu target, operated at 40 kV and 40 mA) was used. It operated at a scanning rate of $4° \cdot min^{-1}$ and scanned continuously across an angle range of 30°–100°. The microstructure characterization of steels was carried out using Phenom Pro scanning electron microscopy (SEM).

Table 1: Measured chemical compositions (wt.%) and density (g·cm^{-3}) of the studied steels

Steels	Mn	Al	C	Fe	Density
10Al0.8C	29.6	9.7	0.7	Bal.	6.48
10Al1.0C	27.8	9.9	1.1	Bal.	6.46
10Al1.2C	29.3	10.3	1.2	Bal.	6.43
10Al1.4C	28.2	10.2	1.4	Bal.	6.42
11Al0.8C	28.8	10.9	0.8	Bal.	6.31
11Al1.0C	28.6	11.3	0.9	Bal.	6.30
12Al0.8C	27.3	12.3	0.8	Bal.	6.26
12Al1.0C	29.8	12.4	1.0	Bal.	6.24

Prior to the SEM characterization, samples were electro-polished in a solution consisting of 10vol.% perchloric acid and 90vol.% alcohol, operated at 18 V for 15 s. To examine the nano-precipitates in steels, a JEM-2100F field emission TEM, operated at 200 kV, was employed. TEM specimens were prepared through twin-jet electrolytic polishing at approximately −25 °C and 40 V, using a solution consisting of 10vol.% perchloric acid and 90vol.% alcohol. Room temperature tensile tests were performed at a strain rate of 1×10^{-3} s^{-1} using an MTS Criterion Model 44 mechanical property tester, with at least four repetitions were carried out for each steel strip. The tensile samples were prepared with dimensions of 20 mm×4 mm×1 mm.

To clarify the influence of Al and C on the formation of κ-carbides, first-principles calculations were performed using all spin-polarized density functional theory (DFT) [39-42], as implemented in the Materials Studio software. These calculations were executed in reciprocal space, employing the special k-point method in the first Brillouin zone as per the Monkhorst-Pack scheme. For the FCC structure, 2×2×2 supercells were used, and a 3×3×3 k-points grid was applied within the Brillouin zone for these supercells. The projector augmented waves (PAW) formalism in conjunction with generalized gradient approximation (GGA) was used for calculating the exchange-correlation potential [43]. The plane wave cut-off energy was set to 400 eV, and geometric optimization was achieved using the Broyden-Fletcher-Goldfarb-Shanno (BFGS) algorithm [43], ensuring adequate atomic relaxation. The convergence criteria were: the energy difference between consecutive self-consistent calculation cycles was below 1×10^{-5} eV·atom^{-1}, the force on each atom was not greater than 0.03 eV·Å^{-1}, and the internal stress did not exceed 0.03 GPa. To examine the effects of Al and C content on κ-carbide formation, variations in total energies and lattice parameters of $Fe_{24}Al_8C_8$ were calculated as the number of Al atoms and C atoms were changed in the supercells.

3 Results

3.1 Structures and mechanical properties of steels with different C content

3.1.1 Microstructures and nano-precipitates

Figure 1 presents the XRD patterns of 10Al*y*C steels, in which the steels are composed of austenite (γ) and ferrite (δ). With the increase of C content, there is a slight decrease in the diffraction peak intensity of δ(110) at 2θ=44.1°, indicating a decrease in ferrite content. The microstructure of 10Al*y*C low-density steels by SEM is shown in Fig. 2, revealing irregularly shaped ferrite (identified with a yellow arrow) distributes uniformly within the austenite matrix. Analysis of ferrite content in the SEM images [Figs. 2(a–d)], conducted with Image-Pro Plus (IPP) software reveals that the volume fraction of ferrite in 10Al0.8C, 10Al1.0C, 10Al1.2C and 10Al1.4C steels is determined to be 27.3vol.%, 22.6vol.%, 13.4vol.%, and 8.7vol.%, respectively. Previous research by Yoo et al. [8] indicated that when the C content exceeded 1.0wt.%, Fe-28Mn-9Al-C low-density steels exhibited a single-phase austenite structure. However, this study shows that even with C content above 1.0wt.%, a significant amount of ferrite remains in the low-density steels. It should be due to the high cooling rate during near-rapid solidification, preserving high-temperature ferrite at room temperature.

To investigate the influence of C content on κ-carbide precipitation, TEM characterization was carried out on the κ-carbides in 10Al*y*C steels. Figure 3 shows dark-field (DF) images of the κ-carbides and corresponding selected area electron diffraction (SAED) patterns taken along $[001]_\gamma$ zone axis. Nano-scale κ-carbides are found to be dispersed within the austenite matrix, with the SAED patterns revealing coherent characteristics between the κ-carbides and austenite. Analysis using IPP software reveals that the mean size of κ-carbides in 10Al0.8C, 10Al1.0C, 10Al1.2C, and 10Al1.4C steels is measured to be 9.6 nm, 11.0 nm, 15.7 nm, and 38.2 nm, respectively. The content of κ-carbides in the steels is determined to be 10.2vol.%, 12.6vol.%, 15.2vol.%, and 29.8vol.%, respectively. Additionally, the intensity of the diffraction spots corresponding to κ-carbides increases proportionally with the rise in C content from 0.8wt.% to 1.4wt.%. Notably, the κ-carbides precipitated in 10Al1.4C

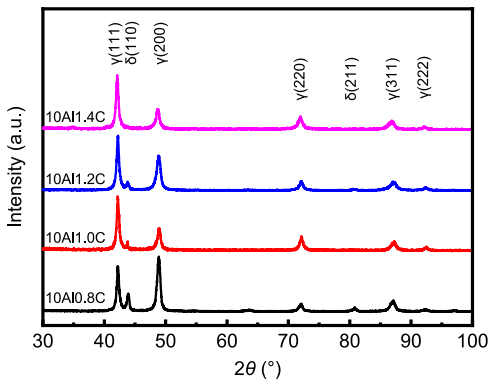

Fig. 1: XRD patterns of 10Al*y*C low-density steels

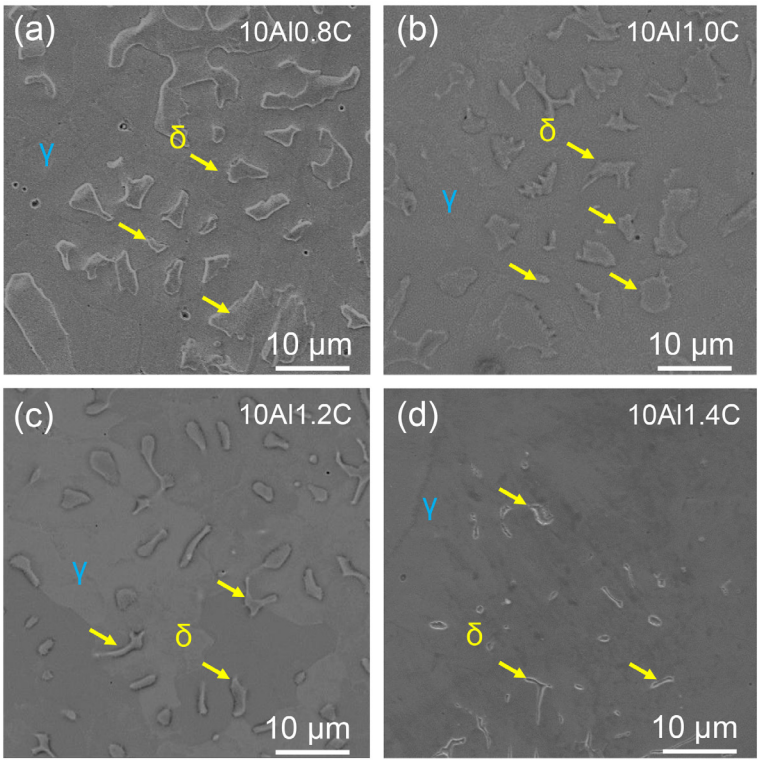

Fig. 2: SEM images of 10Al*y*C low-density steels (a–d)

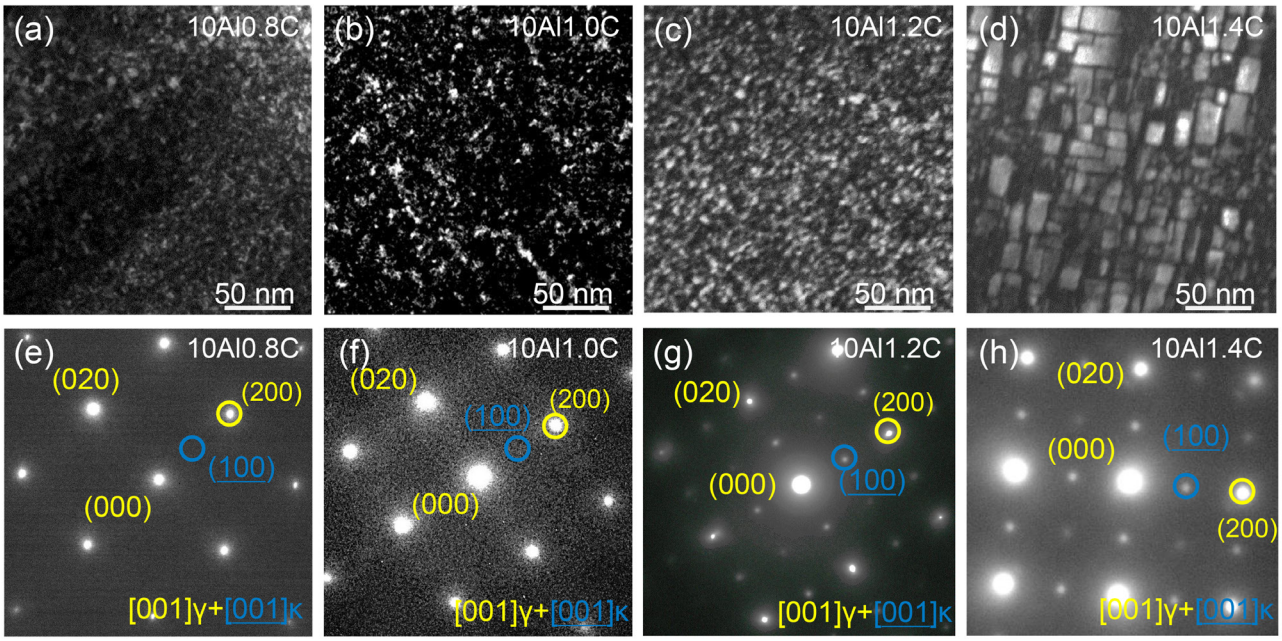

Fig. 3: TEM DF images of κ-carbides in 10Al0.8C (a), 10Al1.0C (b), 10Al1.2C (c), and 10Al1.4C (d) steels with corresponding SAED patterns (e–h) along $[001]_{\gamma}$

steel exhibit a distinct blocky morphology. The evolution of the average size and volume fraction of κ-carbides in 10Al*y*C steels is summarized in Fig. 4.

3.1.2 Mechanical properties

Figure 5 shows the micro-hardness evolution and engineering stress-strain curves of 10Al*y*C steels. With the rise in C content from 0.8wt.% to 1.4wt.%, the micro-hardness of steels increases from 298 HV to 398 HV, as shown in Fig. 5(a). Figure 5(b) shows the engineering stress-strain curves of 10Al*y*C steels, with corresponding mechanical properties detailed in Table 2. The strengthening influence of C content on low-density steel is evident, as seen by the significant increase in yield strength (YS) and ultimate tensile strength (UTS) as C content rises from 0.8wt.% to 1.4wt.%. Specifically, the yield strength increases from 571 MPa to 1,175 MPa, marking a 604 MPa increment, while the ultimate tensile strength increases from 782 MPa to 1,224 MPa, marking a 442 MPa increment. It is worth noting that due to the precipitation of large-sized κ-carbides in 10Al1.4C steel, its yield strength is

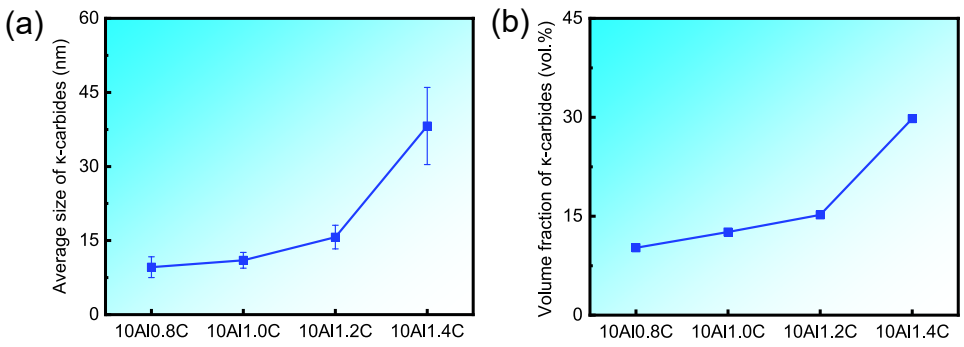

Fig. 4: Average size (a) and volume fraction (b) of κ-carbides in 10Al*y*C low-density steels

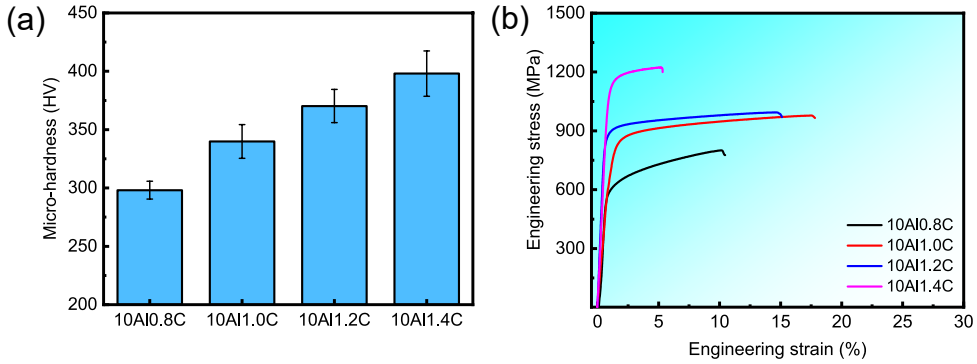

Fig. 5: Micro-hardness (a) and engineering stress-strain curves (b) of 10Al*y*C low-density steels

Table 2: Mechanical properties of 10Al*y*C low-density steels

Steels	YS (MPa)	UTS (MPa)	TEL (%)
10Al0.8C	571±21	782±14	10.1 ± 3.6
10Al1.0C	841±13	962±17	17.3±2.1
10Al1.2C	862±24	994±10	16.1±4.3
10Al1.4C	1,175±12	1,224±23	6.2±1.7

significantly increased by 313 MPa compared to 10Al1.2C steel. However, the ductility of 10Al*y*C low-density steels initially increases and then decreases with increasing C content. The total elongation (TEL) of 10Al1.4C steel is only 6.2%.

3.2 Structures and mechanical properties of steels with different Al content

3.2.1 Microstructures and nano-precipitates

Figure 6 displays the XRD patterns of *x*Al0.8C and *x*Al1.0C low-density steels. In comparison to the 10Al*y*C low-density steels, the phase constitution of the low-density steels with varying Al content is still dominated by austenite and ferrite, with no new phase observed in the XRD patterns. Additionally, as the Al content increases, the intensity of ferrite diffraction peaks gradually intensifies. Compared to 10Al steels, there is a significant decrease in austenite peak intensity of 11Al and 12Al steels. This means that higher Al content reduces the volume fraction of austenite. Figure 7 presents the SEM images of *x*Al0.8C and *x*Al1.0C low-density steels. As the Al content increases, the ferrite shape becomes more irregular and the size and content of ferrite significantly increase. Quantitative measurement using IPP software shows that the ferrite content is 27.3vol.%, 31.8vol.%, 36.8vol.%, 22.6vol.%, 28.7vol.%, and 33.2vol.% for 10Al0.8C, 11Al0.8C, 12Al0.8C, 10Al1.0C, 11Al1.0C, and 12Al1.0C steels, respectively. During the near-rapid solidification process, the δ-ferrite firstly forms in the liquid phase, and then transforms into austenite as the temperature decreases [44]. Due to Al being an ferritic element, an increase in Al content would expand the phase region of δ-ferrite [37], resulting in more ferrite remaining during the rapid cooling, thereby increasing the content and size of ferrite at room temperature.

Figure 8 shows the TEM characterization on κ-carbides in *x*Al0.8C and *x*Al1.0C low-density steels. In the *x*Al0.8C steels, as the Al content increases from 10wt.% to 11wt.% and 12wt.%, the mean size of κ-carbides increases from 9.6 nm to 10.2 nm and 11.4 nm, respectively, as depicted in Figs. 3(a), 8(a), and 8(b). For the steels with 1.0wt.% C, the mean size of κ-carbides in the 10Al1.0C, 11Al1.0C, and 12Al1.0C steels is 11.0 nm, 13.6 nm, and 17.6 nm, respectively, as shown in Figs. 3(b), 8(c), and 8(d). The volume fraction of κ-carbides in 11Al0.8C, 11Al1.0C, 12Al0.8C, and 12Al1.0C steels is measured to be 12.9vol.%, 15.9vol.%, 17.8vol.%, and 19.2vol.%, respectively. The mean size and content of κ-carbides are increased with the increase in Al content, as summarized in Fig. 9.

3.2.2 Mechanical properties

Figure 10 shows the micro-hardness of *x*Al0.8C and *x*Al1.0C steels. The data show a notable increase in micro-hardness as the Al content rises. For the *x*Al0.8C steels, the micro-hardness

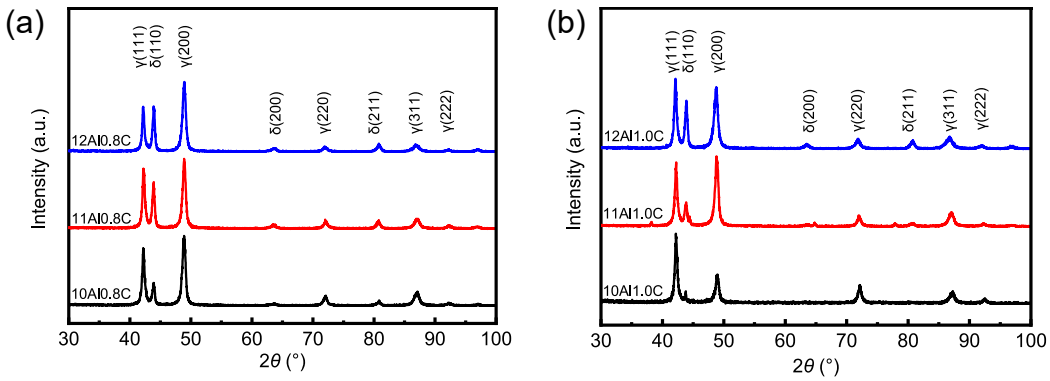

Fig. 6: XRD patterns of *x*Al0.8C (a) and *x*Al1.0C (b) low-density steels

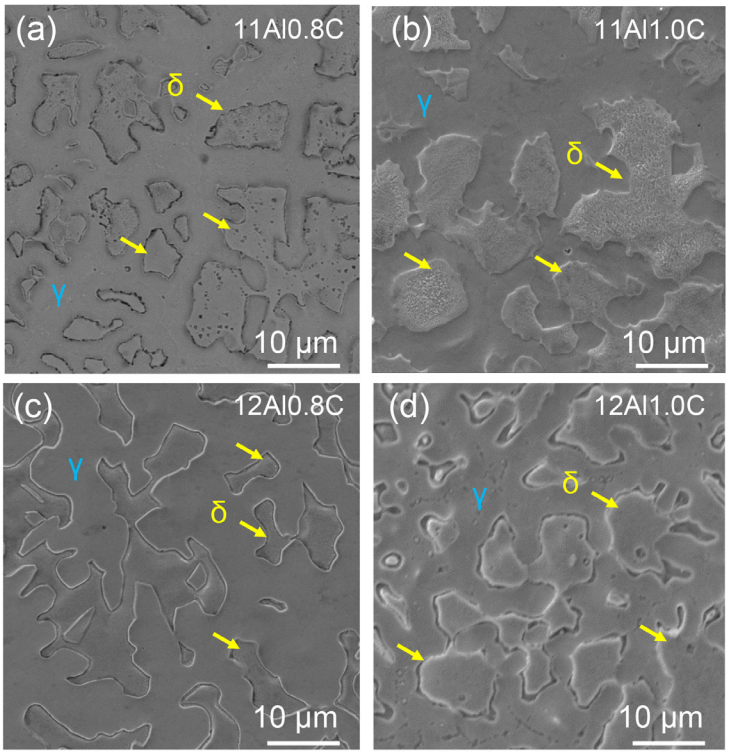

Fig. 7: SEM images of *x*Al0.8C and *x*Al1.0C low-density steels (a–d)

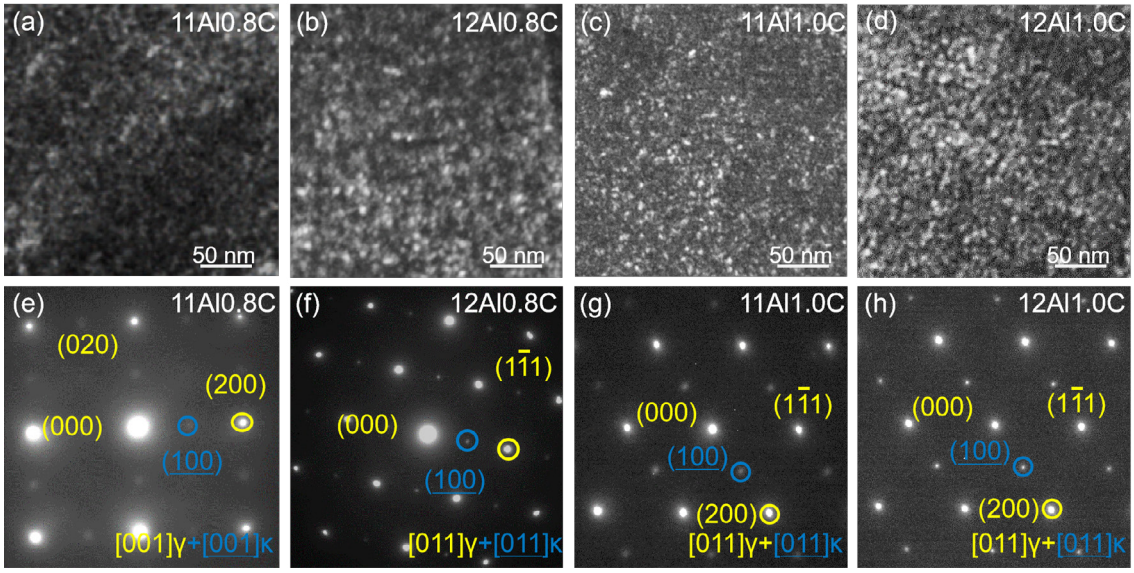

Fig. 8: TEM DF images of κ-carbides in 11Al0.8C (a), 12A0.8C (b), 11Al1.0C (c), and 12Al1.0C (d) steels with corresponding SAED patterns (e–h) along $[001]_\gamma$ or $[011]_\gamma$

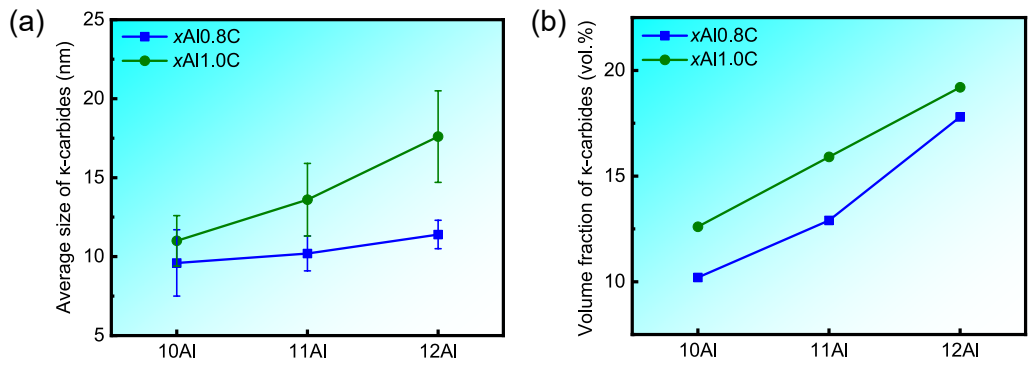

Fig. 9: Average size (a) and volume fraction (b) of κ-carbides in steels with different Al content

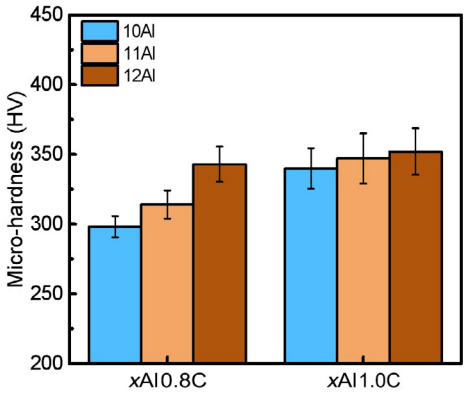

Fig. 10: Micro-hardness of *x*Al0.8C and *x*Al1.0C low-density steels

value increases from 298 HV to 342 HV with increasing the Al content. However, when the C content reaches 1.0wt.%, the impact of increasing Al content on micro-hardness diminishes significantly.

Figure 11 displays the engineering stress-strain curves of *x*Al0.8C and *x*Al1.0C steels, revealing that the yield strength of steels increases with an increase in Al content. Interestingly, the impact of increased Al content on the strength enhancement is less pronounced in low-density steels compared to those with varying C content. Specifically, comparing to 10Al0.8C steel, the yield strength of 11Al0.8C and 12Al0.8C steels increases by about 126 MPa and 236 MPa, respectively. Similarly, for 11Al1.0C and 12Al1.0C steels, their yield strength increment is roughly 48 MPa and 105 MPa compared to 10Al1.0C steel.

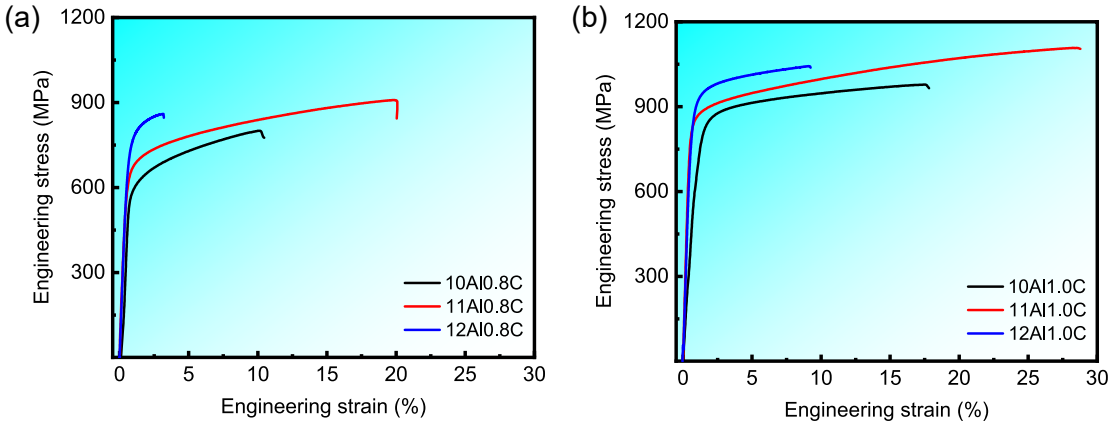

Fig. 11: Engineering stress-strain curves of *x*Al0.8C (a) and *x*Al1.0C (b) low-density steels

Table 3: Mechanical properties of *x*Al0.8C and *x*Al1.0C low-density steels

Steels	YS (MPa)	UTS (MPa)	TEL (%)
10Al0.8C	571±21	782±14	10.1±3.6
11Al0.8C	697±12	903±21	19.4±4.7
12Al0.8C	807±21	861±34	3.1±0.7
10Al1.0C	841±13	962±17	17.3±2.1
11Al1.0C	889±31	1,100±9	26.4±3.3
12Al1.0C	946±18	1,039±12	9.0±3.1

In the low-density steels with varying Al content, the impact of increasing C content on enhancing yield strength diminishes as Al content increases. For the steels containing 10wt.% Al, the increase of C content from 0.8wt.% to 1.0wt.% results in a yield strength increment of 270 MPa. However, for the steels with 11wt.% and 12wt.% Al, the strength increments between the steels with C content of 0.8wt.% and 1.0wt.% are 192 MPa and 139 MPa, respectively. Concurrently, the ductility of the low-density steel initially increases and then decreases with the rise in Al content. When the C content is 0.8wt.% and 1.0wt.%, the 11Al steels exhibit the best ductility, 19.4% and 26.4%, respectively, while the 12Al steels exhibit the poorest ductility, 3.1% and 9.0%, respectively.

4 Discussion

4.1 Impact of Al and C content on κ-carbide precipitation

Quantitative analyses were performed on the average size and volume fraction of κ-carbides in Fe-28Mn-*x*Al-*y*C low-density steels to clarify the influence of Al and C content on the precipitation behavior of κ-carbides, as shown in Fig. 12. Figure 12(a) displays the relationship and fitting curve between average sizes of κ-carbide and Al and C content in different steels. To demonstrate the accuracy of the fitting curves, the coefficient of determination (R^2) for the fitting curves was calculated. The value of R^2 greater than 0.8 and closer to 1 indicates a higher accuracy of the fit curves. The calculated range of R^2 for this work is found to be between 0.85 and 0.95, suggesting a relatively higher accuracy, as shown in Fig. 12. The slope of the fitting curve for C content is significantly greater than that of the fitting curve for Al content, suggesting that the impact of C content on the average size of κ-carbides is much more pronounced compared to that of Al content. Even with an increase in Al content up to 12wt.%, the size of κ-carbides in steels with 1.0wt.% C content remains below 20 nm. However, in the 10Al1.4C steel, the average size of κ-carbides reaches 38.2 nm, as depicted in Fig. 4. The pronounced effect of C element on κ-carbides is also evident in the evolution of κ-carbide volume fraction, as shown in Fig. 12(b). As the C content increases, the volume fraction of κ-carbides rises from 10.2vol.% in 10Al0.8C steel to 29.8vol.% in 10Al1.4C steel. For the steels with C content of 0.8wt.% and 1.0wt.%, as the Al content increases from 10wt.% to 12wt.%, the volume fraction of κ-carbides only increases by 7.6vol.% and 6.6vol.%, respectively.

To understand the impact of Al and C content on κ-carbide precipitation, thermodynamic calculations were carried out on Fe-28Mn-*x*Al-*y*C system steels. Using FactSage 8.3 software, the Gibbs free energy of κ-carbide between 400 °C and 800 °C was calculated for 10Al*y*C and *x*Al0.8C steels, as depicted in Figs. 13(a) and (b). A lower energy of κ-carbide indicates higher stability, facilitating its precipitation. Results reveal that with increasing Al or C content, the Gibbs free energy of κ-carbide consistently decreases, suggesting that higher Al or C levels enhance κ-carbide precipitation. This corresponds to the TEM results shown in Figs. 3 and 8. Notably, the impact of C content on the Gibbs free energy of κ-carbide is more pronounced. Linear fitting analysis was performed on the relationship between Gibbs free energy of κ-carbide and Al and C content at 500 °C and 700 °C, as shown in Figs. 13(c) and (d). Across different temperature ranges, the slope of fitting lines corresponding to C content is consistently lower than that of Al content, implying that the increase in C content leads to a greater reduction in the Gibbs free energy of κ-carbide compared to Al content. Therefore, the increase in C content results in a greater driving force for the formation of κ-carbides.

In addition, our previous work has found that the ordered nuclei of κ-carbide could form directly in the disordered austenite, following the nucleation and growth mechanism [45]. Based on the classical nucleation theory, the minimum activation energy barrier for the nucleation of κ-carbides can be expressed as [46]:

$$\Delta G^{*}=\frac{16\pi E_{\kappa/\gamma}^{3}}{3\left(\Delta G_{\mathrm{V}}-\Delta G_{\mathrm{S}}\right)^{2}} \tag{1}$$

where $E_{\kappa/\gamma}$ is the interfacial energy between κ-carbides and austenite, with a value of 0.2 J·m^{-2} [47], ΔG_{V} is the chemical driving force of κ-carbides, and ΔG_{S} is the elastic strain energy. Among them, ΔG_{S} can be expressed as [46]:

$$\Delta G_{\mathrm{S}}=\frac{E\delta^{2}\left(c-c_{0}\right)^{2}}{1-v} \tag{2}$$

with lattice mismatch of $$\delta=\frac{a_{\gamma}-a_{\kappa}}{a_{\kappa}} \tag{3}$$

where E is the Young's modulus, c is the nucleation composition, c_0 is the nominal composition, v is the Poisson's ratio, a_κ is the lattice constants of κ-carbide, and a_γ is the lattice constant of austenite. Generally, the elastic strain energy (ΔG_{S}) is proportional to the square of lattice mismatch between κ-carbides and austenite [46]. Therefore, a lower lattice mismatch corresponds to a reduction in elastic strain energy.

In this work, it is challenging to determine the lattice mismatch between κ-carbide and austenite in steels with varying Al and C content by direct XRD measurement,

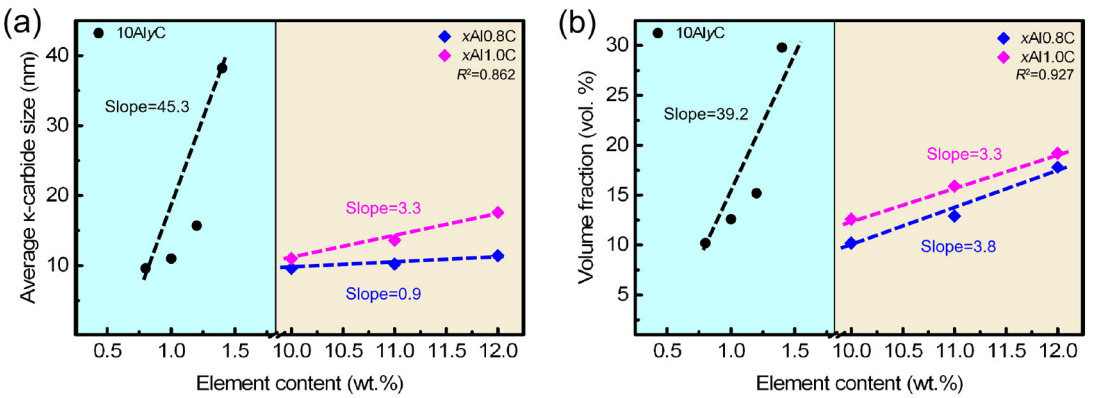

Fig. 12: Relationship and fitting curve between average size (a) and volume fraction (b) of κ-carbides and Al and C content in different steels

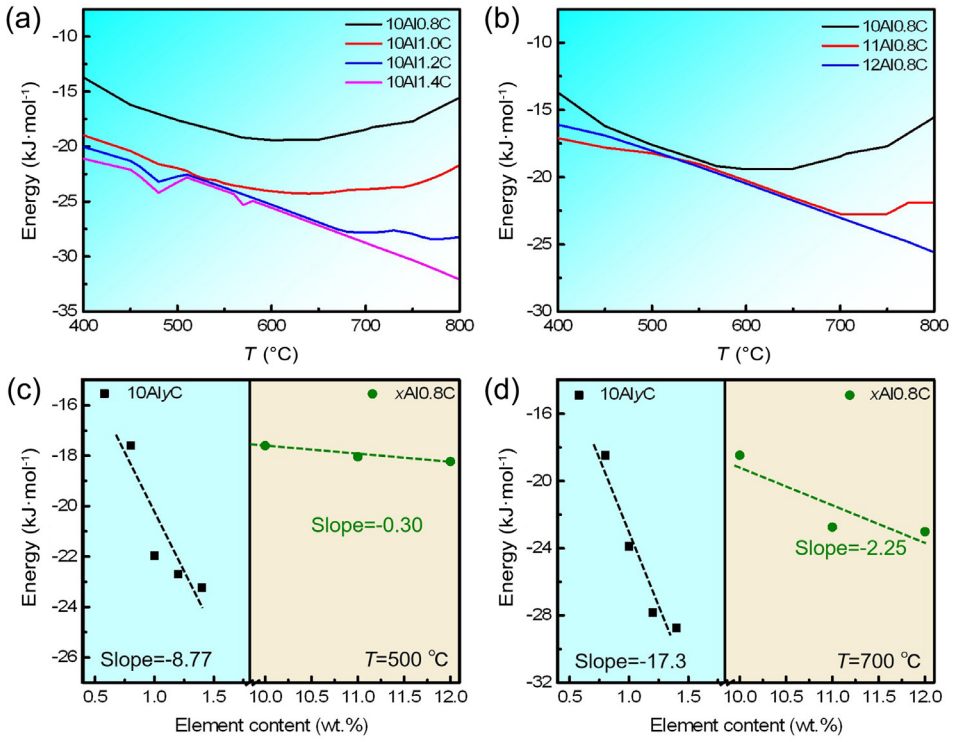

Fig. 13: Gibbs energy of κ-carbides in 10Al*y*C (a) and *x*Al0.8C (b) low-density steels at different temperatures, and fitting curves between Gibbs free energy of κ-carbides and Al and C content at 500 °C (c) and 700 °C (d)

because of the indistinct diffraction peak of κ-carbide in Figs. 1 and 6. The austenite lattice constants obtained from XRD measurements are shown in Table 4. During the X-ray diffraction measurement process, the BBDD monochromator was utilized to monochromatize the radiation, thereby preserving only the necessary K-alpha radiation. The acquired data were then smoothed and subtracted from the background by Origin software. Subsequently, the processed data were analyzed by JADE software and PDF cards. Following this, the austenite peak was fitted to determine the corresponding lattice constant.

First-principles calculations were further performed using Materials Studio to analyze the impact of Al and C content on the theoretical lattice mismatch between the two phases. The supercell lattice constant was set to 0.716 nm from XRD, and each supercell was subjected to at least three calculations to ensure the accuracy under the condition of vivo modulus with 250 GPa. Then, it performed by CASTEP (a procedure for computing quantum mechanics from initial states based on density functional methods) to figure out the difference of lattice constants with different Al and C content. Figure 14(a) shows the 2×2×2 FCC-Fe structure cells (austenite, a_γ=0.341 nm) supercell structure with 32 Fe atoms, whereas Fig. 14(b) shows the supercell structure of κ-carbide (Fe_3AlC, a_κ=0.367 nm). To elucidate the impact of Al and C content on the austenite lattice constant, supercell structures with an approximate ratio of real Al and C content in Fe-28Mn-*x*Al-*y*C steels were constructed, based on the fundamental FCC structure. The 10Al0.8C steel, for instance, matches a supercell structure with 6Al atoms (18.14at.%) and 1C atoms (3.26at.%) added. The specific correspondence between Al and C content and supercell structure is also shown in Table 4. After optimization, the changes in austenite lattice constant with increasing Al or C content are shown in Figs. 14(c) and (d), as well as Table 4.

Table 4: Atomic numbers of Al and C atoms, lattice constant, and lattice mismatch in *x*Al*y*C steels by experiment and calculation

Steels	Corresponding Al and C atom number	Lattice constant by XRD (nm)	Lattice constant by calculation (nm)		Lattice mismatch between κ-carbide and austenite
		a_γ	a_γ	a_κ	δ
10Al0.8C	6Al1C	0.350	0.347	0.367	0.054
11Al0.8C	7Al1C	0.353	0.350	0.367	0.046
12Al0.8C	8Al1C	0.358	0.352	0.367	0.041
10Al1.4C	6Al2C	0.355	0.349	0.367	0.049

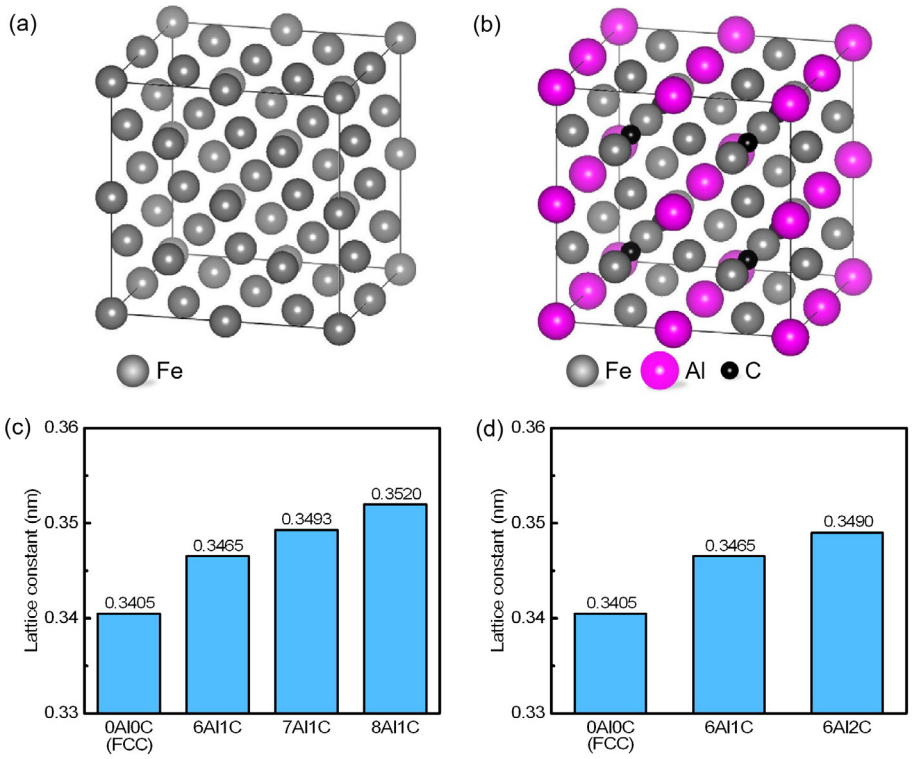

Fig. 14: Calculated supercell of FCC-Fe structure (a) and κ-carbide (Fe_3AlC) (b), and calculated lattice constant of FCC-Fe with different numbers of Al (c) and C (d) atoms

Obviously, the lattice constant of the FCC structure is raised by increasing the number of Al and C atoms, and the impact of increasing the number of Al atoms is somewhat stronger. The increase of C atoms reduces the lattice mismatch between κ-carbide and austenite from 0.054 to 0.049, while the increase of Al atoms reduces the lattice mismatch between the two phases from 0.054 to 0.041, as shown in Table 4. The reason for the difference between the calculated values and experimental values by XRD is that the calculated values are theoretical calculations based on FCC-Fe, while the experimental values are affected by the solid solution of C atoms and κ-carbides. Although the increase in Al content results in a smaller lattice mismatch, which is more favorable for the κ-carbide nucleation, the increase in C content has a greater effect on the Gibbs free energy of κ-carbides, which in turn greatly enhances the precipitation and growth of κ-carbides in austenite, as shown in Figs. 3 and 8.

4.2 Strengthening effect analysis of κ-carbides

As mentioned above, the size and volume fraction of κ-carbides show a nearly linear increase with a higher Al and C content, which is significantly influential in their ability to strengthen low-density steels [29]. Computational analyses were conducted on steels with varying Al and C content to understand the precipitation strengthening of κ-carbides. Due to the coherent characteristics between κ-carbides and austenite, variations in the size of κ-carbides can lead to different interactions between κ-carbides and dislocations during plastic deformation, i.e. particle shearing and bypassing mechanisms [48, 49]. Research undertaken by Kim et al. [50] established a critical radius of 13.4 nm for the shearing and bypassing mechanisms. However, multiple studies have shown that κ-carbides with a size of around 20 nm could still be cut by dislocations during deformation [24, 48]. Furthermore, Yao et al. [48] calculated a critical radius of 38 nm for the shearing and bypassing mechanisms for κ-carbides, which was supported by TEM characterization.

In this work, the average size of intragranular κ-carbides in the 10Al0.8C, 10Al1.0C, 10Al1.2C, and 10Al1.4C steels is 9.6 nm, 11.0 nm, 15.7 nm, and 38.2 nm, while in 11Al0.8C and 12Al0.8C is 10.2 nm and 11.4 nm, respectively, as shown in Figs. 4 and 9. Based on the computational model by Yao et al. [48], when the κ-carbide size is less than 38 nm, it can be cut by dislocations. Normally, when dislocations cut through particles, in order to maintain the ordered structure of κ-carbide and avoid the formation of antiphase boundary (APB), a pair of super-partial dislocations would travel through the κ-carbide together [48]. When the κ-carbide size is less than 10 nm, such as 10Al0.8C steel, the super-partials are weakly coupled, and the strength contribution by these κ-carbides can be given by

$$\sigma_p = \frac{M}{N}\frac{\gamma_{APB-\kappa}}{b}\sqrt{V_f}\left[\sqrt{\frac{12\gamma_{APB-\kappa}r}{\pi Gb^2}} - \sqrt{V_f}\right] \quad (4)$$

where M is the Taylor factor (3.06) [47], b is the Burgers vector taken to be 0.25 nm [46], G is the shear modulus of the austenite matrix, which is 70 GPa [47], N is the number of pile-up dislocations that contributes to shearing the intragranular precipitates (N=8 [50, 51]), r is the radius of κ-carbides, and V_f is the volume fraction of κ-carbides [52], where $\gamma_{APB-\kappa}$ is the APB energy generated with κ-carbide shearing ($\gamma_{APB-\kappa}$=350 mJ·m^{-2} [48]). When the κ-carbide size is between 10 nm and 38 nm, the

super-partials are strongly coupled, and the strength contribution by κ-carbides can be given by

$$\sigma_p = \frac{M}{N}\sqrt{\frac{3}{2}}\left(\frac{Gb}{r}\right)\sqrt{V_f}\,\frac{2w}{\sqrt{\pi^3}}\left[\frac{2\pi\gamma_{APB-\kappa}r}{wGb^2}-1\right]^{\frac{1}{2}} \quad (5)$$

where w is a dimensionless constant with a value of 2 and $\gamma_{APB-\kappa}$ becomes to 700 mJ·m^{-2} [48]. When the κ-carbide size is larger than 38 nm, the interaction between κ-carbides and dislocations follows the by passing mechanism. The strength contribution by κ-carbides by passing can be expressed as [52]

$$\sigma_p = 0.538Gb\left(\frac{V_f^{\frac{1}{2}}}{D}\right)\ln\left(\frac{D}{2b}\right) \quad (6)$$

where D is the diameter of κ-carbides.

Based on the above computational model, the strength contribution by intragranular κ-carbides is calculated to be 238.3 MPa, 383.9 MPa, 404.4 MPa, and 583.4 MPa in 10Al0.8C, 10Al1.0C, 10Al1.2C, and 10Al1.4C steels, and 420.8 MPa and 474.3 MPa in 11Al0.8C and 12Al0.8C, as shown in Fig. 15. It can be observed that although different mechanisms are followed, the strengthening effect of κ-carbides still significantly increases with their size and content, and results in a maximum strength increment of 583 MPa.

In this study, the 12Al0.8C steel has the highest ferrite content, reaching 36.8vol.%. Therefore, it is necessary to discuss the influence of the ferrite phase and nanoscale κ-carbides on the mechanical properties. The ferrite phase formed from the high-temperature liquid metal during sub-rapid solidification, contributes less to the yield strength, as demonstrated in previous experiments [53]. Ferrite is a softer phase compared to austenite, the nano-hardness of austenite exceeds twice than that of ferrite in previous studies [53]. The contribution of ferrite to yield strength is less than that of κ-carbides. The strength contribution of κ-carbides in 10A0.8C, 10Al1.0C, 10Al1.2C, and 10Al1.4C low-density steels is calculated to be 41.7%, 45.7%, 46.9%, and 49.6%, and in 11Al0.8C and 12Al0.8C is 60.4% and 58.7%, as shown in the tables inside of Fig. 15. The analysis of strength contribution demonstrates that, despite the increase of ferrite content due to the rise in Al content, the proportion of strength contribution from κ-carbides within the total yield strength is significantly amplified to over 50%. This observation suggests that κ-carbides impart a greater contribution to the strength of the material than ferrite.

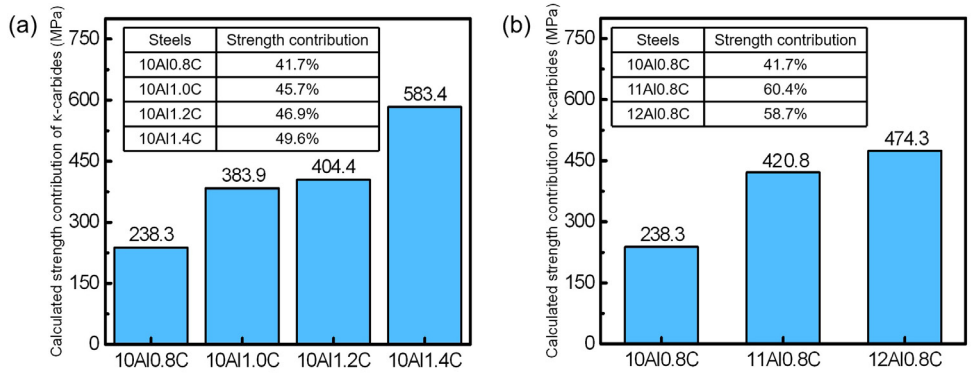

Fig. 15: Calculated strength contribution of κ-carbides in steels with different Al and C content (a, b)

5 Conclusions

Fe-28Mn-xAl-yC steels were designed to investigate the impact of varying Al and C content on the precipitation behavior of κ-carbide and its strengthening effect in high-Mn low-density steels. The specific conclusions are as follows:

(1) The microstructure of Fe-28Mn-xAl-yC low-density steels exhibits a combination of austenite matrix and ferrite. For the 10AlyC steels, an increase in C content from 0.8wt.% to 1.4wt.% results in a decrease in ferrite content from 27.3vol.% to 8.7vol.%. However, increasing Al content has the opposite effect on ferrite content, with the ferrite content in 12Al0.8C and 12Al1.0C steels reaching 36.8vol.% and 33.2vol.%, respectively.

(2) The increase of Al and C content promotes the precipitation and growth of κ-carbides, with C exhibiting a more pronounced effect. In the 10AlyC steels, increasing C content from 0.8wt.% to 1.4wt.% leads to an increase in the average size of κ-carbides from 9.6 nm to 38.2 nm, and the volume fraction of κ-carbides from 10.2vol.% to 29.8vol.%. In addition, among the steels with a C content of 1.0wt.%, the 12Al1.0C steel has the highest κ-carbide content and the largest average size, at 17.6 nm and 19.2vol.%, respectively.

(3) First-principles calculations demonstrate that both the increase in Al and C content could reduce the lattice mismatch between austenite and κ-carbide, favoring κ-carbide nucleation. Furthermore, thermodynamic calculations reveal that the increase in C content results in a greater reduction in the Gibbs free energy of κ-carbide compared to Al content, leading to a stronger driving force for κ-carbide formation. Therefore, the increase in C content has a more significant promoting effect on the precipitation of κ-carbides.

(4) The increase in Al and C content significantly enhances the yield strength of low-density steels by promoting the κ-carbide precipitation. Increasing C content from 0.8wt.% to 1.4wt.% in 10AlyC steels results in a strength increase of 604 MPa. The

maximum strength contribution by intragranular κ-carbides in 10Al1.4C steel could reach 583 MPa. Similarly, increasing Al content from 10wt.% to 12wt.% in the *x*Al0.8C steels, the strength is rose by 236 MPa, the strength contribution by intragranular κ-carbides in 12Al0.8C steel could reach 474 MPa.

Acknowledgments

This work was financially supported by the National Natural Science Foundation of China (Nos. 52301058 and 52271034), the China Postdoctoral Science Foundation (No. 2023M732183), the Postdoctoral Fellowship Program of CPSF (No. GZB20230399), the Key scientific and technological project in Ningbo City (No. 2022Z056). This work was supported by the Independent Research Project of State Key Laboratory of the Advanced Special Steel, Shanghai Key Laboratory of Advanced Ferrometallurgy, Shanghai University (SKLASS 2023-Z12), and the Science and Technology Commission of Shanghai Municipality (No. 19DZ2270200). The authors would like to express their sincere thanks to the staff support at the Instrumental Analysis & Research Center at Shanghai University.

Conflict of interest

The authors declare that they have no known competing financial interests or personal relationships that could have appeared to influence the work reported in this paper.

References

[1] Seede R, Whitt A, Ye J, et al. A lightweight Fe-Mn-Al-C austenitic steel with ultra-high strength and ductility fabricated via laser powder bed fusion. Materials Science and Engineering: A, 2023, 874: 145007.
[2] Rana R (ed.). High-performance ferrous alloys. Springer International Publishing, Cham, 2021.
[3] Rahnama A, Kotadia H, Clark S, et al. Nano-mechanical properties of Fe-Mn-Al-C lightweight steels. Scientific Reports, 2018, 8: 9065.
[4] Ikhmayies S, Li B, Carpenter J, et al. Characterization of minerals, metals, and materials 2016. Springer International Publishing, Cham, 2016.
[5] Kim H, Suh D, Kim N. Fe-Al-Mn-C lightweight structural alloys: A review on the microstructures and mechanical properties. Science and Technology of Advanced Materials, 2013, 14: 014205.
[6] Chen S, Rana R, Haldar A, et al. Current state of Fe-Mn-Al-C low density steels. Progress in Materials Science, 2017, 89: 345–391.
[7] Frank C. Current trends in automotive lightweighting strategies and materials. Materials, 2021, 14(21): 6631.
[8] Yoo J, Hwang S, Park K. Factors influencing the tensile behavior of a Fe-28Mn-9Al-0.8C steel. Materials Science and Engineering: A, 2009, 508: 234–240.
[9] Ha M, Koo J, Lee J, et al. Tensile deformation of a low density Fe-27Mn-12Al-0.8C duplex steel in association with ordered phases at ambient temperature. Materials Science and Engineering: A, 2013, 586: 276–283.
[10] Lu W, Zhang X, Qin R. κ-carbide hardening in a low-density high-Al high-Mn multiphase steel. Materials Letters, 2015, 138: 96–99.
[11] Frommeyer G, Brüx U. Microstructures and mechanical properties of high-strength Fe-Mn-Al-C light-weight triplex steels. Steel Research International, 2006, 77: 627–633.
[12] Moon J, Park S, Jang J, et al. Atomistic investigations of κ-carbide precipitation in austenitic Fe-Mn-Al-C lightweight steels and the effect of Mo addition. Scripta Materialia, 2017, 127: 97–101.
[13] Han D, Ding H, Liu D G. The microstructures and tensile properties of aged Fe-*x*Mn-8Al-0.8C low-density steels. Materials Science and Technology, 2020, 36: 681–689.
[14] Kong H, Liu C. A review on nano-scale precipitation in steels. Technologies, 2018, 6: 36.
[15] Haase C, Zehnder C, Ingendahl T, et al. On the deformation behavior of κ-carbide-free and κ-carbide-containing high-Mn light-weight steel. Acta Materialia, 2017, 122: 332–343.
[16] Chen P, Zhang F, Zhang Q, et al. Precipitation behavior of κ-carbides and its relationship with mechanical properties of Fe-Mn-Al-C lightweight austenitic steel. Journal of Materials Research and Technology, 2023, 25: 3780–3788.
[17] Banis A, Gomez A, Dutta A, et al. The effect of nano-sized κ-carbides on the mechanical properties of an Fe-Mn-Al-C alloy. Materials Characterization, 2023, 205: 113364.
[18] Moshiri A, Zarei-Hanzaki A, Charkhchian J, et al. Room temperature deformation mechanisms of a Fe-Mn-Al-C steel. Journal of Materials Research and Technology, 2023, 26: 4696–4705.
[19] Zhang G, Wang S, Li B, et al. Achieving high strength and ductility in Fe-Mn-Al-C austenitic steel via vanadium microalloying and aging. Journal of Materials Research and Technology, 2023, 24: 8443–8457.
[20] Gomez A, Banis A, Avella M, et al. The effect of κ-carbides on high cycle fatigue behavior of a Fe-Mn-Al-C lightweight steel. International Journal of Fatigue, 2024, 184: 108306.
[21] An Y F, Chen X P, Mei L, et al. Precipitation transformation pathway and mechanical behavior of nanoprecipitation strengthened Fe-Mn-Al-C-Ni austenitic low-density steel. Journal of Materials Science & Technology, 2024, 174: 157–167.
[22] Chin K, Lee H, Kwak J, et al. Thermodynamic calculation on the stability of $(Fe,Mn)_3AlC$ carbide in high aluminum steels. Journal of Alloys and Compounds, 2010, 505: 217–223.
[23] Park S, Park J, Cho K, et al. Effect of Mn and C on age hardening of Fe-Mn-Al-C lightweight Steels. Metals and Materials International, 2019, 25: 683–696.
[24] Wu Z, Ding H, An X, et al. Influence of Al content on the strain-hardening behavior of aged low density Fe-Mn-Al-C steels with high Al content. Materials Science and Engineering: A, 2015, 639: 187–191.
[25] Kim M, Kang Y. Development of thermodynamic database for high Mn-high Al steels: Phase equilibria in the Fe-Mn-Al-C system by experiment and thermodynamic modeling. Calphad, 2015, 51: 89–103.
[26] Wu Z, Tang Y, Chen W, et al. Exploring the influence of Al content on the hot deformation behavior of Fe-Mn-Al-C steels through 3D processing map. Vacuum, 2019, 159: 447–455.
[27] Xu Z, Liang J, Chen Y, et al. Sintering of a porous steel with high-Mn and high-Al content in vacuum. Vacuum, 2022, 196: 110746.
[28] Burja J, Šetina Batič B, Balaško T. Kappa carbide precipitation in duplex Fe-Al-Mn-Ni-C low-density steel. Crystals, 2021, 11: 1261.
[29] Zambrano O. A general perspective of Fe-Mn-Al-C steels. Journal of Materials Science, 2018, 53: 14003–14062.

[30] Wang H, Wang C, Liang J, et al. Effect of alloying content on microstructure and mechanical properties of Fe-Mn-Al-C low-density steels. Materials Science and Engineering: A, 2023, 886: 145675.
[31] Ren P, Chen X, Mei L, et al. Intragranular brittle precipitates improve strain hardening capability of Fe-30Mn-11Al-1.2C low-density steel. Materials Science and Engineering: A, 2020, 775: 138984.
[32] Kalashnikov I, Acselrad O, Shalkevich A, et al. Chemical composition optimization for austenitic steels of the Fe-Mn-Al-C system. Journal of Materials Engineering and Performance, 2000, 9: 597–602.
[33] Kim J, Lee S, DeCooman B. Effect of Al on the stacking fault energy of Fe-18Mn-0.6C twinning-induced plasticity. Scripta Materialia, 2011, 65: 363–366.
[34] Moon J, Park S, Jang J, et al. Investigations of the microstructure evolution and tensile deformation behavior of austenitic Fe-Mn-Al-C lightweight steels and the effect of Mo addition. Acta Materialia, 2018, 147: 226–235.
[35] Moon J, Ha H, Park S, et al. Effect of Mo and Cr additions on the microstructure, mechanical properties and pitting corrosion resistance of austenitic Fe-30Mn-10.5Al-1.1C lightweight steels. Journal of Alloys and Compounds, 2019, 775: 1136–1146.
[36] Liu M, Li X, Zhang Y, et al. Precipitation of κ-carbide in a V-containing austenite-based lightweight steel. Metallurgical and Materials Transactions: A, 2022, 53: 1231–1243.
[37] Gutierrez-Urrutia I. Low density Fe-Mn-Al-C steels: Phase structures, mechanisms and properties. Iron and Steel Institute of Japan, 2021, 61: 16–25.
[38] Baligidad R, Prasad K. Effect of Al and C on structure and mechanical properties of Fe-Al-C alloys. Materials Science and Technology, 2007, 23(1): 38–44.
[39] Achmad T, Fu W, Chen H, et al. First-principles calculations of generalized-stacking-fault-energy of Co-based alloys. Computational Materials Science, 2016, 121: 86–96.
[40] Park N, Choi J, Cha P, et al. First-principles study of the interfaces between Fe and transition metal carbides. Journal of Physical Chemistry: C, 2013, 117: 187–193.
[41] Kresse G, Furthmüller J. Efficiency of ab-initio total energy calculations for metals and semiconductors using a plane-wave basis set. Computational Materials Science, 1996, 6(1): 15–50.
[42] Perdew J, Burke K, Ernzerhof M. Generalized gradient approximation made simple. Physical Review Letters, 1996, 77: 3865–3868.
[43] Fischer T, Almlof J. General methods for geometry and wave function optimization. Journal of Physical Chemistry, 1992, 96: 9768–9774.
[44] Liu L, Li C, Yang Y, et al. A simple method to produce austenite-based low-density Fe-20Mn-9Al-0.75C steel by a near-rapid solidification process. Materials Science and Engineering: A, 2017, 679: 282–291.
[45] Zhang J, Liu Y, Hu C, et al. The effect of Cr content on intragranular κ-carbide precipitation in Fe-Mn-Al-(Cr)-C low-density steels: A multiscale investigation. Materials Characterization, 2022, 186: 111801.
[46] Li Z M, Körmann F, Grabowski B, et al. Ab initio assisted design of quinary dual-phase high-entropy alloys with transformation-induced plasticity. Acta Materialia, 2017, 136: 262–270.
[47] Kim C, Terner M, Lee J, et al. Partitioning of C into κ-carbides by Si addition and its effect on the initial deformation mechanism of Fe-Mn-Al-C lightweight steels. Journal of Alloys and Compounds, 2019, 775: 554–564.
[48] Yao M, Welsch E, Ponge D, et al. Strengthening and strain hardening mechanisms in a precipitation-hardened high-Mn lightweight steel. Acta Materialia, 2017, 140: 258–273.
[49] Liu M, Li X, Zhang Y, et al. Multiphase precipitation and its strengthening mechanism in a V-containing austenite-based low density steel. Intermetallics, 2021, 134: 107179.
[50] Welsch E, Welsch D, Hafez-Haghighat S, et al. Strain hardening by dynamic slip band refinement in a high-Mn lightweight steel. Acta Materialia, 2016, 116: 188–199.
[51] Lee J, Kim H, Jeong K, et al. Prediction of precipitation kinetics and strengthening in FeMnAlC lightweight steels. Journal of Materials Research and Technology, 2021, 14: 2897–2908.
[52] Lee D, Kim J, Lee S, et al. Microstructures and mechanical properties of Ti and Mo micro-alloyed medium Mn steel. Materials Science and Engineering: A, 2017, 706: 1–14.
[53] Zhang J, Hu C, Liu Y, et al. Microstructure, mechanical properties and deformation behavior of Cr-containing triplex low-density steels with different C content. Journal of Materials Research and Technology, 2023, 23: 6075–6089.